



Synthetic inhibition of the SUMO pathway by targeting the SAE1 component via TAK-981 compound impairs growth and chemosensitizes embryonal and alveolar rhabdomyosarcoma cell lines

Silvia Codenotti¹ · Volker M. Lauschke^{2,3,4,5} · Emma V. Casella¹ · Daniel C. Andersson² · Alessandro Fanzani¹ · Stefano Gastaldello²

Received: 12 March 2025 / Accepted: 5 June 2025
© The Author(s) 2025

Abstract

Rhabdomyosarcoma (RMS) is a highly aggressive pediatric soft tissue sarcoma with limited therapeutic options, particularly for cases resistant to conventional treatments. The SUMOylation pathway, which plays a key role in regulating the cell cycle, apoptosis, and transcription, has emerged as a potential therapeutic target in RMS. Elevated levels of SUMO1 and SUMO2/3 conjugates in RMS cell lines, compared to normal human skeletal muscle cells, underscore the association between upregulated SUMOylation and aggressive cancer phenotypes. Understanding these molecular underpinnings is critical for the development of innovative and effective treatments. The investigation encompassed transcriptomic and protein analyses to profile SUMOylation pathway components across alveolar and embryonal RMS subtypes, aiming to identify heterogeneity that could guide personalized therapy approaches. TAK-981, a small molecule that selectively inhibits the SUMOylation of target proteins, was evaluated in combination with chemotherapeutic agents for additive or synergistic effects. Additionally, its impact on radiosensitivity and key signaling pathways, such as AKT, ERK and CAV1 phosphorylation, was assessed to elucidate its mechanism of action. Transcriptomic and proteomic analyses revealed distinct expression profiles of SUMOylation pathway components across RMS subtypes, highlighting heterogeneity that could guide personalized therapeutic strategies. Notably, SAE1 protein was overexpressed in RMS tissues and cells, positioning it as a potential biomarker for this cancer. Its activity was effectively counteracted by TAK-981, a SUMO inhibitor that demonstrated significant therapeutic potential by suppressing RMS cell proliferation and migration, and enhancing the cytotoxic effects of chemotherapeutic agents actinomycin D and doxorubicin. However, TAK-981 did not increase radiosensitivity, suggesting its selective action through chemical inhibition mechanisms. Mechanistically, TAK-981 reduced phosphorylation of key signaling proteins, including AKT, ERK and CAV1, which are critical for RMS cell survival. The findings of this study establish TAK-981 as a promising therapeutic agent for RMS. The results also provide foundational insights into the role of SUMOylation associated with the new biomarker SAE1 in RMS and its subtypes, paving the way for the development of personalized treatment strategies that leverage SUMO pathway inhibition.

Keywords Rhabdomyosarcoma · FP-RMS/ARMS · FN-RMS/ERMS · SUMO · TAK-981

Abbreviations

PTM(s)	Post-translational modification(s)	UBC9	Ubiquitin conjugating enzyme 9
SENPs(s)	Sentrin-specific proteases	PIASs	Protein inhibitor of activated STAT superfamily
SUMO	Small Ubiquitin-like Modifier	pAKT	Phosphorylated AKT
SUMO E1	SUMO-activating enzyme E1	pERK	Phosphorylated ERK
SAE1/2	SUMO activating enzyme subunits ½	pCAV1	Phosphorylated Caveolin-1
SUMO E2	SUMO-conjugating enzyme E2	hSKM	Human Skeletal Muscle Cells
SUMO E3	SUMO ligase E3	PML	Promyelocytic Leukemia Protein

Extended author information available on the last page of the article

Introduction

Rhabdomyosarcoma (RMS) is a rare and aggressive form of cancer that originates in the soft tissues, specifically in skeletal muscle cells. This malignancy primarily affects children and adolescents, though it can also occur in adults. RMS is thought to arise from embryonic muscle cells that fail to differentiate into mature muscle cells, leading to the formation of cancerous tissues [1]. Based on the presence or absence of the chromosomal translocations t(2;13) or t(1;13) [2, 3], RMS is classified molecularly into fusion-positive RMS (FP-RMS/alveolar) or fusion-negative RMS (FN-RMS/embryonal), respectively, giving rise to chimeric factors that play a large role in RMS malignancy [4, 5]. Among the six RMS histotypes, the alveolar and embryonal are the most common. The alveolar subtype with an incidence of 32% [6], tends to occur in older children and is generally more aggressive whereas the embryonal subtype is twice as common [6], often found in younger children and associated with a more favorable prognosis. The symptoms of RMS depend on the location of the tumor but may include swelling, pain, or a lump in the affected area. Common sites for these tumors include the head and neck, genitourinary tract, and extremities [7] [8]. Treatment strategies for RMS typically involve a multidisciplinary approach, combining surgery, chemotherapy, and radiation therapy [9]. Despite advancements in treatment, RMS poses significant challenges, and outcomes can vary.

RMS prognosis varies depending on tumor histotype and status. Patients with low-risk localized disease treated with a multimodal approach have a 5-year survival greater than 70%. The overall survival rate for patients presenting with high-risk metastatic or recurrent disease remains lower than 30% [10, 11].

The Small ubiquitin-like modifier (SUMO) network is a crucial cellular mechanism involved in post-translational modification. SUMOylation and de-SUMOylation are reactions that involve the attachment and removal of the modifiers (SUMO1–2–3–4–5) to proteins, modifying their function, localization, or interaction with other molecules [12–14]. This reaction is dynamic and reversible, playing a significant role in various cellular activities, including gene expression, DNA repair, and cell cycle regulation. Furthermore, the SUMO network has emerged as an appealing target for pharmacological modulation. SUMOylation begins with the activation of SUMO proteins by the enzyme E1, called SUMO-activating enzyme (SAE), a heterodimer composed of SAE1 (SUMO-activating enzyme subunit (1) and UBA2, also known as SAE2 (SUMO-activating enzyme subunit (2)). The activated SUMO is then transferred to the E2 enzyme,

the SUMO-conjugating enzyme (UBC9). Finally, with the help of the E3 enzyme (SUMO ligases-PIAS), SUMOs are conjugated to a lysine residue on the target protein via an isopeptide bond [15, 16]. In contrast, deSUMOylation is primarily carried out by SUMO-specific proteases (SENPs) of the sentrin family, which in humans includes six members (SEN1-3 and SEN5-7) that differ in their tissue specificity and subcellular localization [17]. SENPs cleave the isopeptide bond between SUMO and the target protein, releasing the SUMO molecule from its protein scaffold [18]. Together, SUMOylation and deSUMOylation create a dynamic and reversible regulatory system in cells, which is essential for cellular homeostasis, response to stress, and adaptation to changing environmental conditions [19].

Aberrations in the SUMO network have been implicated in cancer development and progression [20, 21]. Specifically, the SUMO system is known to modulate the activity of several proteins involved in cancer-related pathways, such as those regulating cell cycle progression, apoptosis and DNA repair. In certain cancers such as breast [22], colorectal [23], prostate [24], lung [25], and pancreatic [26], the overexpression of specific SUMO enzymes or changes in the SUMOylation status of proteins may promote tumorigenesis [27]. Conversely, reduced SUMOylation can compromise the activity of certain tumor suppressor proteins such as BRCA1 and PML (Promyelocytic Leukemia Protein) [28]. Understanding these intricacies of the SUMO network and its involvement in cancer biology has prompted research into therapies that target SUMOylation dynamics [29, 30]. In RMS, particularly in alveolar subtypes, SUMOylation may influence the stability, subcellular localization, and activity of oncogenic transcription factors, including PAX3-FOXO1 and PAX7-FOXO1 [31] [32], thereby enhancing their tumor-promoting functions. Additionally, SUMOylation modulates key cellular processes such as cell cycle progression and apoptosis, contributing to uncontrolled proliferation and resistance to cell death.

There has been interest in developing small molecules that can modulate the SUMO pathway such as Spectomycin B1 [33], Ginkgolic Acid [34], and Anacardic Acid [35]. N106 [36] and TAK-981 [37] are compounds that specifically enhance or inhibit SUMOylation.

In this study, we focused on TAK-981 for its selective inhibition of SUMO conjugation that minimizes off-target effects compared to broader drugs and preserves other ubiquitin-like pathways (e.g., ubiquitination or NEDDylation, and in combination with its promising effects described in previous studies in the cancer field [30, 38–40]. We demonstrated that TAK-981 a mechanism-based inhibitor of SAE which forms SUMO–TAK-981 adducts as the inhibitory species within the enzyme catalytic site located in the SAE1 subunit, reduces SUMOylation in alveolar and embryonal

RMS cells in vitro in a dose-dependent manner, causing a reduction in cell proliferation and migration. Our data provide the first evidence that interfering with SUMOylation represents a promising targeted therapeutic approach for RMS, particularly in cases characterized by SUMOylation gain-of-function, supporting the emerging concept that inhibition of this pathway can suppress tumor growth and potentially improve clinical outcomes.

Materials and methods

Chemicals

N-ethylmaleimide (NEM, E1271), sodium chloride (NaCl, Merck 6404), dithiothreitol (DTT, D5545), iodoacetamide (I1149), IGEPAL CA-630 (NP40, I3021), ethylenediaminetetraacetic acid disodium salt dehydrate (EDTA, E4884), sodium deoxycholate monohydrate (DOC, D5670), triton X-100 (T9284), glycine (G-7126), albumin from bovine serum (BSA, A7906), sodium dodecyl sulfate (SDS, L3771), tween-20 (P9416), Trizma base (T93349), actinomycin D (A-9415), and all oligonucleotides for quantitative real-time PCR (Table 1) were purchased from Sigma-Aldrich (St. Louis, MO). Doxorubicin (5927S) was purchased from Cell Signaling Technologies (MA, USA). Subsumstat (TAK-981, HY111789) was purchased from MedChemExpress MCE (Stockholm, Sweden). Complete™ protease inhibitors

cocktail tablets (protease inhibitors) and phosphatase inhibitor cocktail were purchased from Roche Diagnostic (Mannheim, Germany).

Antibodies

The antibodies used for western blot were: rabbit anti-SUMO-1 (Y299, ab32058, 1:4000), rabbit anti-SUMO-2/3 (EPR4602, ab109005, 1:8000), goat anti-UBE21/UBC9 (ab21193, 1:3000), rabbit anti-SAE1 (ab185552, 1:2000), rabbit anti-SAE2 (ab185955, 1:5000), rabbit anti-PIAS1 (ab109388, 1:2000), rabbit anti-SEN1 (ab236094, 1:1000), rabbit anti-SEN3 (ab124790, 1:1000), rabbit anti-SEN5 (ab58420, 1:1000), and polyclonal donkey horseradish peroxidase (HRP)-conjugated anti-goat/sheep IgG (ab6885, 1:5000) from AbCam (Cambridge, UK). Rabbit anti-PIAS4 (Pa5-20,954, 1:3000) from Thermo Fisher Scientific (IL, USA). Rabbit anti-PIAS3 (SC 14017, 1:2000), mouse anti-phospho-Erk1/2 (sc-7383, 1:500), and mouse anti-Erk1/2 (sc-514302, 1:500) from Santacruz Biotechnology, INC. Rabbit anti-ubiquitin (Z0458, 1:6000), polyclonal swine anti-rabbit IgG (P0399), polyclonal rabbit anti-mouse IgG (P0260) Horseradish Peroxidases (HRP) conjugated antibodies (1:5000) from DAKO (Glostrup, Denmark). Rabbit anti-phospho-Akt (#4060, 1:1000), and rabbit anti-Akt (#4691, 1:1000) from Cell Signaling Technologies (MA, USA). Mouse anti-phospho-Caveolin-1 (611,338, 1:500) from BD (New Jersey, USA). Goat anti-SEN2 (1:6000

Table 1 Primers sequences used for qPCR

Transcripts	Primer FWD 5'-3'	Primer REV 5'-3'	Size (bp)
SUMO1	TGGACAGGACAGCAGTGAGA	CCCCGTTTGTTCCTGATAA	110
SUMO2	GGACAGGATGGTTCTGTGGT	TGCTGCTGGAACACATCAAT	110
SUMO3	GAACGACCACATCAACCTGA	TGTCCTCATCCTCCATCTCC	110
SAE1	GACTCATCGGAGACCACCAT	CATCCTCGCTGTAGCTGTCA	110
UBA1	CAAGGAGAAGAAGCCAATGC	CGTGACAAAATCCATTGCAG	110
UBC9	ACGTGTATCCTTCTGGCACA	TTGTGCTCGAACCTTTTCT	105
PIAS1	CAGCGACTTCTCTCCATCC	TTGATCAGTTCGTCCAGCAG	105
PIAS2	TGTTTCATCAAGCCCACAA	CTTCTTGAGGGCAACTGGTC	105
PIAS3	AGTTTCGATGCTGCCCTTTA	CCTTCTGGGTTTCATTGGA	105
PIAS4	TGCTTTGATGCCGTGTTCTA	GCTTGGTTCCTTCTCTGCAC	105
TRAF7	GAAAGAATGCGAGCACATCA	GAACGCAGAAAGGCAATCTC	105
RANBP2	GAACGTGGGATAGGCAATGT	CTGGTTTGGGCAATTCATCT	105
TOPORS	GAGGACAAGGAGTGCGATGT	GTGGAGATGGCAATGGTCTT	105
SEN1	AAAGACTCCGCTCTTCACCA	CGGGCTCGAGAGTCATAAAC	105
SEN2	GGAAGCAATGGCCTACTCAG	CCACGGGTGATTCTGTAACCT	105
SEN3	AAAAGCACCTCGCTGACATT	ATCCTCTGCCATGAGAGCAC	110
SEN5	GAGGGGTCTTCACATCCAGA	GCCCAAGTCTTTGCTGAAG	110
SEN6	GAACCAAGCAACGGAGAGTC	GGGTCATCCTGATCCTCTGA	110
SEN7	TGCTTCAGTCTCTCTTTCC	ACTTCTGAACGGGTCCAGTG	110
RNF4	AACCCCTGAGATTTCTTGG	CACAGCTGTCAGCATGGTCT	105
GAPDH	AACCCATCACCATCTTCCAG	GTGGTTCACACCCATCACAA	100

WB) antibodies were a gift from Dr. Ron T. Hay (College of Life Sciences, Dundee University, Dundee, UK). The specificity of the commercial antibodies has been validated in our previous publications [41, 42] or from laboratories that provided other antibodies.

Cell culture

Primary Human Skeletal Muscle Cells isolated from different skeletal muscles from adult single donors (human skeletal myoblasts, hSKM, A12555) from Thermo Fischer Scientific. Alveolar FP-RMS: RH30, RH41; embryonal FN-RMS: RH36, RD12 a clone of RD and RD were cultured in Dulbecco's Modified Eagle's Medium 6046 (DMEM-high glucose, 5.5 mM, 308–340 mOs/Kg with L-Glutamine G6392) supplemented with 10% 56 °C heat-inactivated Foetal Bovine/Calf Serum (FBS) and 1X 100 IU/ml of penicillin and streptomycin (Thermofischer scientific). Cells were harvested and washed with cold PBS in the presence of 0.2 M iodoacetamide. When required, different concentrations of TAK-981 (0.1, 1, 10, 50, 100 nM) were added to the cell cultures as indicated. Stocks were prepared in DMSO, and the final working concentration did not exceed 0.01% v/v, with no observed DMSO-induced cytotoxicity.

Cell lysates

Cells or myotubes were lysed in RIPA buffer (25 mM Tris–Cl pH 7.5, 50 mM NaCl, 0.5% NP40, 0.1% SDS, 0.5% DOC, 1 mM DTT, 20 mM NEM and fresh added protease and phosphatase inhibitors). A syringe with 29G needle was used to mechanically disrupt genomic DNA. Lysates were clarified at 10,000 g for 15 min at 4 °C. Protein concentration (DC Protein Assay Kit, Bio-Rad) was determined on the clear supernatants.

Immunoblotting

Desired concentrations of cell lysates were denatured for 10 min at 95 °C in loading buffer (NuPage 4X, Reducing Agent 10X, Invitrogen, Carlsbad, CA) and loaded in acrylamide Bis–Tris 4–12% gradient gels (Invitrogen, Carlsbad, CA). After transfer onto PVDF membranes (Merck Millipore, Bedford, MA) for 60 min at 0.34 A, the filters were blocked in TBS-T solution (50 mM Tris–Cl, 150 mM NaCl, 0.1% Tween-20 and 5% non-fat milk, pH 7.6), and incubated with specific primary antibodies overnight at 4 °C, following an incubation with the appropriate horseradish peroxidase-conjugated secondary antibodies for 1 h at room temperature. Proteins were visualized by chemiluminescence (ECL, GE Healthcare, Uppsala, Sweden), detected by the ChemiDoc MP Imaging System (Bio-Rad Laboratory, CA), and chemiluminescence intensity was analyzed only

for non-saturated bands using the corresponding imaging analysis software, ImageJ version 5.0. To minimize membrane and sample waste, some proteins were detected either by cutting membranes according to molecular weight or by stripping with Western Blot Stripping Buffer (91,925, Cell Signaling), followed by reblocking and reprobing with specific antibodies.

Quantitative real time PCR (qPCR)

SUMO component transcript abundance was assayed by qPCR using the primers listed in Table 1 (Sigma-Aldrich, St. Louis, MO, USA) and previously designed with PRIMER3 software (http://biotools.umassmed.edu/bioapps/primer3_www.cgi). RNAs were extracted using the GeneJET RNA purification Kit (K0731, Thermo Fisher Scientific, Lithuania) and subjected to DNase I treatment (EN0521, Thermo Fisher Scientific, Lithuania). The correspondent cDNAs were produced using both oligo (dT)18 and random primers using the RevertAID H Minus First strand cDNA synthesis Kit (K1632, Thermo Fisher Scientific, Lithuania). qPCR reactions were performed with 100 ng of cDNA template using the SYBR Green Master Mix (A25741, Life Technologies, Carlsbad, CA, USA) in a 20 µl of final volume. The analysis was performed with QuantStudio 3 Real-Time PCR Systems, with the following cycling program: initial 50 °C 2 min, denaturation 95 °C 10 min, followed by 40 cycles of 95 °C for 15 s and 60 °C for 1 min. A final step of melting curve between 65 °C and 90 °C, 1 °C/sec temperature speed was incorporated. Relative fold change relative to the house-keeping control gene (*GAPDH*) was calculated as $2^{-\Delta C_t}$ ($\times 1000$) where: $\Delta C_t = C_t(\text{target}) - C_t(\text{GAPDH})$, according to the Minimum Information for Publication of Quantitative Real-Time PCR Experiments (MIQE) guideline. We validated that similar results were obtained using two other commonly used reference genes, *HPRT* and *Rpl38*. The gene expression based on the geometric average from these genes was similar and we thus decided to keep *GAPDH* as reference gene. Data are presented as mean and \pm standard deviation from in triplicate analyses.

Cell migration assay

Cell migration was quantified through wound healing assay. Cells seeded in 12-well plates (4×10^4) formed confluent monolayers that were pre-treated for 2 h with TAK-981 or DMSO and then wounded by scraping the cells with a 200 µl-sterile micropipette tip. After 8 and 24 h from wound, cells were fixed with 3% paraformaldehyde (PFA)/PBS solution (20 min, 4 °C) and stained with crystal violet solution (0.2% crystal violet/20% methanol/PBS) (10 min, RT). Images of wound healing were acquired at different time-points by an inverted light microscope (Olympus IX50;

Olympus, Tokyo, Japan) using cellSens Software (Olympus, Tokyo, Japan). The extent of wound repair was quantified by measuring the healed area using ImageJ software and normalized to initial wound size. Results were presented as percentage of repaired area with respect to time 0 h.

Cell proliferation assay

Cell proliferation was quantified through measurement of crystal violet incorporation. Cells were seeded in 96-well plates (2×10^3) and treated with TAK-981 or DMSO for 24, 48 or 72 h after seeding. At the indicated time points, cells were fixed with 3% PFA/PBS solution (20 min, 4 °C) and stained with crystal violet solution (0.2% crystal violet/20% methanol/PBS) (10 min, RT). Cells were washed and resuspended in 1% sodium dodecyl sulfate (SDS)/PBS solution. Plates were shaken until complete dissolution was achieved and then absorbance was measured by reading the plate at 595 nm emission wavelength.

Clonogenic assay

Cells were seeded into 6-well plates in triplicate (at a density of 1000 cells/well) to evaluate the clonogenic capacity of the cells. After 10 days, colonies were fixed with 3% PFA/PBS solution (20 min, 4 °C) and stained with crystal violet solution (0.2% crystal violet/20% methanol/PBS) (10 min, RT). Wells were washed with deionized water and pictures of colonies were taken. Then, the dye was solubilized in 1% SDS/PBS solution. Plates were shaken until complete dissolution of the cells, and then absorbance was measured by reading the plate at 595 nm emission wavelength.

Cell viability assay

Cell viability was quantified by measuring the incorporation of MTT (3-[4,5-dimethyl-2-thiazolyl]-2,5-diphenyl-2H-tetrazolium bromide). Cells were seeded in 96-well plates (2×10^3) and then treated with the indicated compounds after 24 h. 48 h after treatment, cells were incubated with cell medium containing 0.5 mg/mL MTT dissolved (3.5 h, 37 °C) before solubilization in DMSO. Absorbance was measured by reading the plate at 540 nm emission wavelengths.

Ionizing radiation treatment

Ionizing radiation treatment was performed at room temperature on subconfluent cells pre-treated or not with the indicated compounds for 2 h at 4 Gray (Gy) doses using a 6 MV photon beam Linear Accelerator (dose rate of 2 Gy/min). The culture dishes were on top of a 1.5 cm plexi-glass block using a Source-Dish distance of 100 cm and a

20×20 cm field. Post-irradiated cells were processed for clonogenic assays.

Bioinformatic analysis

RNA sequencing (RNA-seq) data of an RMS patient cohort of FN-RMS ($n = 66$) and FP-RMS ($n = 35$) samples compared to normal skeletal muscle samples ($n = 5$) were extracted from GEO (accession number GSE108022) [2]. RNA-seq data were preprocessed and normalized using the iDEP.96 tool (Prof. Xijin Ge, South Dakota State University, Brookings, SD, USA) [43], and gene expression was calculated as Log2 Counts per Million (CPM). Data were analyzed and plotted using either GraphPad Prism 8.0 software (GraphPad Software, San Diego, CA, USA) and Qlucore Omics Explorer (Lund, Sweden).

Principal component analysis (PCA) and heatmaps were generated in Qlucore Omics Explorer (Lund, Sweden). Data shown in heatmaps was mean-centered sigma-normalized. Samples were sorted using k-means hierarchical clustering.

Statistical analysis

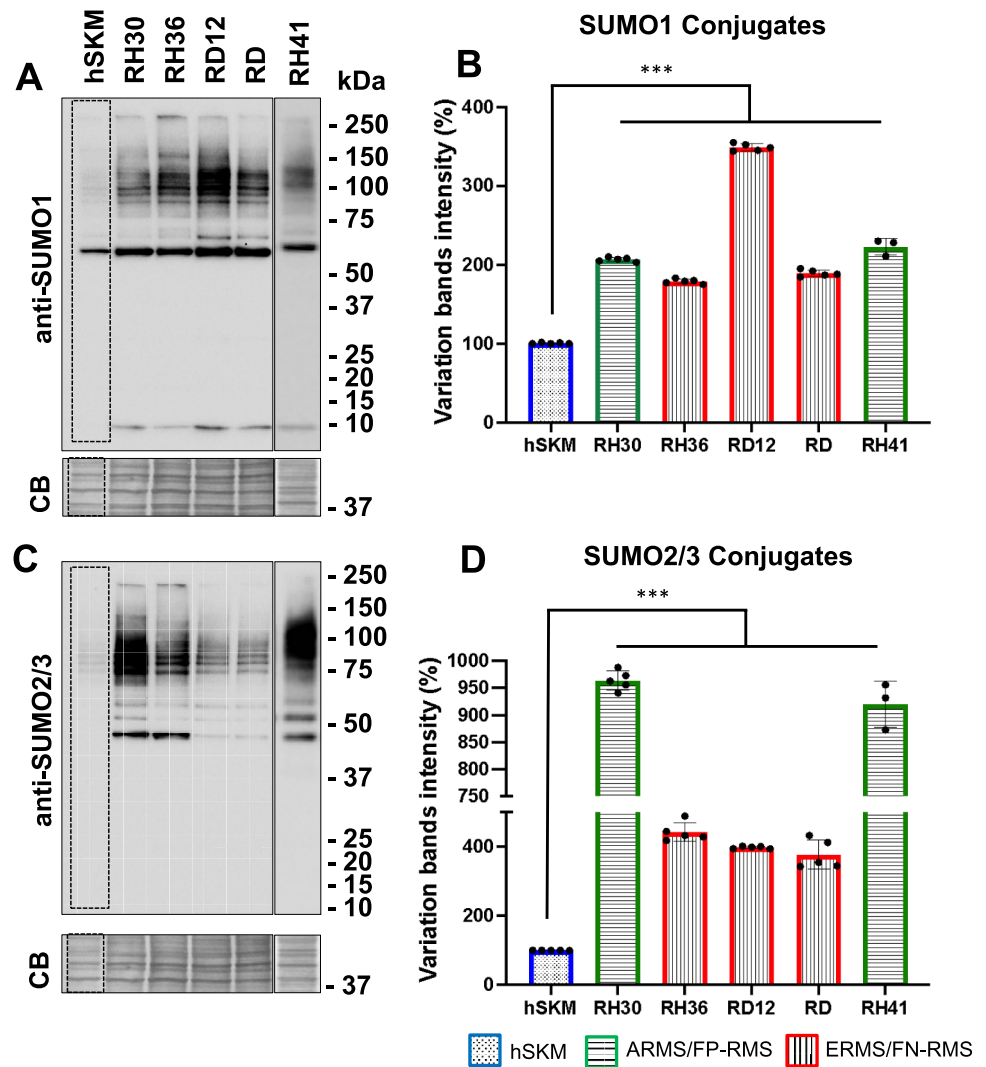
All statistical analyses were performed using GraphPad Prism 8.0 software, with data expressed as mean \pm standard deviation (SD). Statistical significance was determined using unpaired Student's t-test, one-way analysis of variance (ANOVA) followed by post-hoc Tukey's test. Two-sided unpaired t-tests were applied to analyze the difference between two or multiple groups. A p-value < 0.05 was considered statistically significant.

Results

Differential SUMOylation in RMS cell lines

To assess the SUMOylation status, we analyzed global conjugation of SUMO1 and SUMO2/3 in various RMS cell lines, including alveolar FP-RMS cell lines RH30, RH41 (Fig. 1, green columns), embryonal FN-RMS cell lines RH36, RD12, RD (Fig. 1, red columns). These RMS cell lines were compared to normal human skeletal muscle (hSKM) cells, (Fig. 1, blue columns). In hSKM, low levels of SUMO1 and SUMO2/3-conjugated proteins were observed, with a faint pattern of conjugation across a wide molecular weight range (Fig. 1). In contrast, many RMS cell lines showed a marked increase in SUMO1 and SUMO2/3-conjugated proteins, particularly in RH30, RH41, RH36, RD12 and RD where a robust accumulation of high molecular weight SUMO-conjugated proteins was observed, indicative of increased SUMOylation activity (Fig. 1A,C). These effects were specific to SUMO as

Fig. 1 SUMOylation profile in different cell lines. Representative western blots of human skeletal muscles (hSKM), alveolar FP-RMS (RH30, RH41) and embryonal FN-RMS (RH36, RD12, RD) cell lysates probed with anti-SUMO1 (A) and anti-SUMO2/3 (C) antibodies showed distinct patterns of SUMO1 and SUMO2/3 conjugates. For each sample, the quantifications of the SUMO1 and SUMO2/3 conjugates were determined by measuring the band intensity within the dashed areas, normalized to the corresponding total loading protein (Coomassie blue—CB) and the variations, in percentage, were referenced to the hSKM as control (SUMO1 conjugates, B; SUMO2/3 conjugates, D). Molecular weight markers (kDa) are indicated on the right. All data are presented as the mean \pm standard deviation from five independent experiments, except for RH41, $n = 3$. Statistics: ***: $p < 0,001$



the ubiquitin protein profile displayed a consistent pattern in all cells analyzed (Supplementary Fig. 1A and B). Quantification of SUMO1 conjugates showed the highest level in RD12 cells, with nearly a threefold increase in band intensity relative to hSKM, while RH30, RH41, RH36 and RD displayed approximately two-fold increases (Fig. 1B). Quantification of SUMO2/3 conjugates revealed an almost tenfold increase in RH30 and RH41 compared to hSKM cells, with RH36, RD12 and RD showing significant increases of 4- to fivefold (Fig. 1D) suggesting potential heterogeneity in SUMOylation pathways within RMS subtypes. These findings indicate significant dysregulation of SUMO conjugation in several RMS cell lines compared to normal skeletal muscle, with elevated SUMO1 and SUMO2/3 conjugates in RH30, RH41, RH36, RD12, and RD cells, ($p < 0.001$), suggesting that upregulated SUMOylation may contribute to the pathophysiology of RMS.

Comprehensive analysis of SUMO pathway components across RMS and normal skeletal muscle cells

To investigate the differential profiles of SUMO conjugates, we performed transcriptomic analyses of SUMO moieties and SUMO-related enzymes in RMS cells from three independent cultures per cell line where each cell line exhibited a distinct SUMO transcript signature as shown in the heatmap profile and the dendrogram visually represents the hierarchical clustering of the samples (Fig. 2A). Principal component analysis (PCA) of SUMO transcript profiles further segregated RMS samples from control hSKM, highlighting distinct expression patterns between tumor and normal tissues (Fig. 2B).

To validate these transcriptomic findings, cell lysates were fractionated via SDS-PAGE, and membranes were probed with antibodies specific to the SUMO pathway

components E1 (SAE1, UBA2), E2 (UBC9) and E3 ligases (PIAS1, PIAS3, PIAS4 γ), as well as the deconjugating enzymes SENP1, SENP2, SENP3 and SENP5 (Fig. 2C,D). We observed an overall strong correlation between transcript and protein levels. Specifically, in RH30, RH41, RH36, RD12, and RD cells, SAE1 and deconjugases SENP1, SENP2, SENP3, and SENP5 were overexpressed (3–4 times higher than in hSKM, ($p < 0.001$)), while UBA2 expression was reduced by 40–70%. UBC9 was decreased by 30–80% in embryonal RMS cells ($p < 0.001$). PIAS1 was either greatly reduced or undetectable in all RMS cells ($p < 0.001$), and PIAS3 was reduced only in RH36 ($p < 0.001$). No changes were observed in PIAS4 γ expression.

To extend these findings, we performed gene expression profiling of high-throughput RNA sequencing data from 5 normal muscle from tissues and 101 RMS tumor samples [44] (Fig. 2E). Correlating RMS tumor data with cultured RMS cells, we observed consistent transcriptional changes in the SUMO2/3 moieties and several SUMO enzymes. SUMO2/3 ($p = 0.005$), SAE1 ($p = 0.036$), SENP1 ($p = 0.04$), SENP3 ($p = 0.001$), and SENP5 ($p = 0.002$) were upregulated, PIAS1 ($p = 0.004$) was downregulated; UBA2 ($p = 0.51$) showed a trend of downregulation in both tumor samples and RMS cell lines. These results suggest that alveolar and embryonal RMS cells serve as suitable models for further investigation.

Heat shock stress response to RMS and control cells

The SUMOylation pathway is a critical cellular sensor that detects physiological changes and responds by modulating SUMO-conjugated proteins [45]. In the above experiments, we identified variations in SUMO enzyme levels among RMS cells. To explore how SUMOylation responds to stress, we subjected cells to 43 °C heat shocks for 30 min, followed by recovery at 37 °C for 2 h. In human control muscle, a typical SUMOylation response to heat shock was observed. Western blot analyses confirmed that RMS cells exhibit significantly higher levels of SUMO1- and SUMO2/3-conjugated proteins compared to normal skeletal muscle. During the heat shock, SUMOylated proteins accumulated and after the recovery period SUMOylation returned to baseline levels (Fig. 3A,C). Similar patterns were found for RH36 and RD12 cells. In contrast, RH30, RH41 and RD cells maintained elevated levels of SUMOylated proteins even after the recovery period ($p < 0.001$), (Fig. 3B,D). These results provide functional support for the impaired SUMOylation process in these cells due to the alteration of the SUMO enzymes suggesting a role for SUMOylation in stress responses and cancer progression or survival under adverse conditions.

TAK-981 inhibits SUMO conjugation

TAK-981 is a potent and highly selective first-in-class SUMOylation inhibitor with demonstrated anticancer efficacy and is currently undergoing clinical trials for solid tumors [37, 38]. RMS is a soft tissue cancer, and both alveolar and embryonal RMS cells display an accumulation of SUMOylated proteins compared to human myoblasts. We first evaluated the effects of TAK-981 on control hSKM cells and different RMS cell lines. After 4 h of treatment, a dose-dependent reduction in SUMO1 and SUMO2/3 conjugates was observed in RH36 ($p < 0.05$), RD12 ($p < 0.005$), RD ($p < 0.05$), and hSKM ($p < 0.001$) cells, starting at 1 nM TAK-981. In RH41 cells, an 80% reduction in SUMO1 conjugates was observed at 50 nM TAK-981 ($p < 0.001$), while a similar reduction in SUMO2/3 conjugates required 100 nM ($p < 0.001$). In contrast, RH30 cells showed no significant changes in SUMO conjugation, even at 100 nM TAK-981 (Supplementary Fig. 2). When extending exposures to 72 h, complete SUMO deconjugation was achieved in RH36 and RD12 cells with 1 nM TAK-981 ($p < 0.001$), while in RD and hSKM cells, SUMOylation was completely blocked at 50 nM ($p < 0.001$). In RH41, SUMO1 conjugation was blocked at 1 nM TAK-981 ($p < 0.001$), and the SUMO2 conjugation was inhibited at 50 nM drug ($p < 0.001$). RH30 cells became responsive, showing a 25% reduction at 1 nM TAK-981 and a 50% inhibition at 100 nM; however, RH30 cells remained least the sensitive among the tested cell lines (Fig. 4A,B).

TAK-981 reduces cell migration, proliferation and colony formation of RMS cells

Next, we evaluated the functional consequences of SUMO inhibition. In wound healing assays, all cells exhibited delayed repair compared to DMSO-treated controls with a notable effect observed as early as 8 h after treatment where a dose of TAK-981 0.1 nM for RH36 and 1 nM for RH30 significantly ($p < 0.05$) impaired migration, while a dose of 10 nM TAK-981 was efficient for RH41, RD12 and RD cells ($p < 0.001$), (Supplementary Fig. 3A). After 24 h, control hSKM cells almost fully repaired the wound, with only 50 nM TAK-981 impairing repair by ~20%, ($p < 0.005$). In contrast, RMS cells exhibited significantly impaired migration also with 0.1 nM TAK-981: RH30 ($p < 0.05$), RH36, RD12 and RD ($p < 0.001$). RH41 cells showed > 50% reduction in migration at 1 nM ($p < 0.001$), (Fig. 5A).

Subsequently, we investigated the effect of TAK-981 on cell proliferation after 24, 48, and 72 h of treatment using crystal violet assays (Fig. 5B). A reduction of nearly 30% in cell proliferation was evident after 24 h and 50% after 72 h in RH36, RD12, and RD cells treated with 10 nM TAK-981, ($p < 0.05$). In contrast RH30, RH41 and hSKM cells were

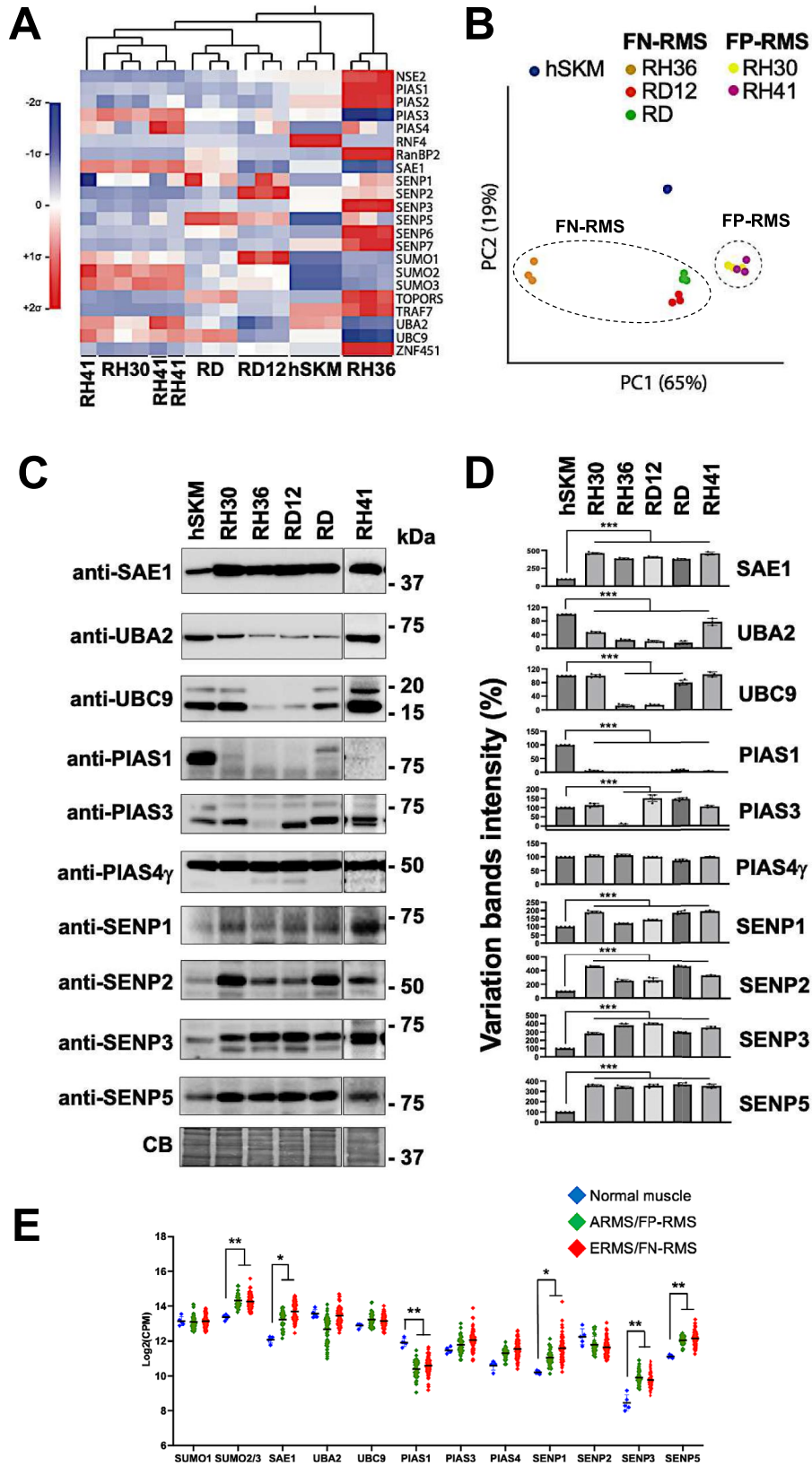


Fig. 2 Transcriptomic analysis of the SUMO moieties (SUMO1, -2, and -3) and the SUMO enzymes from the indicated RMS cell lines. **A** Heat map showing the expression levels of all specified transcripts and normalized to *GAPDH* as housekeeping gene from cell cultures grown and harvested in three independent replicates. Values are represented as mean-centered and sigma-normalized. **B** Principal component analysis of expression data shown in A reveals the formation of distinct clusters, indicating differences in SUMO expression signature among the RMS cells. Three replicates are shown for each condition. Dots are not always clearly visible due to low variabilities within some groups. The two dotted circles indicate clustering of the FN-RMS and FP-RMS cells. **C** Representative western blots of the RMS cells with the indicated antibodies corresponding to validate some SUMO conjugases (SAE1, UBA2, UBC9, PIAS1, PIAS3, PIAS4) and deconjugases (SENP1, SENP2, SENP3, SENP5). Coomassie blue stain (CB) was used as loading control. Molecular weight markers (kDa) are indicated on the right. The complete CB panel for all blots is shown in the uncropped figure file. **D** Quantification of the proteins detected on the corresponding blots. Band intensities were normalized to the corresponding total loading protein (Coomassie blue—CB) and variations were expressed as percentages relative to hSKM as control (100%). All data were presented as the mean \pm standard deviation from five independent experiments, except for RH41, $n=3$. Statistics: ***: $p < 0.001$. **E** Expression levels of genes involved in the SUMOylation and deSUMOylation pathway across different tissue types. The scatter plot presents the log-transformed expression ($\text{Log}_2(\text{CPM})$) of several genes associated with the SUMOylation and deSUMOylation processes, measured in normal muscle from tissue, FN-RMS, and FP-RMS. The data points are color-coded by sample type: blue dots represent normal muscle tissue, green dots represent FP-RMS, red dots represent FN-RMS. Genes displayed along the x-axis include components of the SUMOylation pathway (e.g., SUMO1, SUMO2/3, SAE1, UBA2, UBC9) regulators such as PIAS1–PIAS4, and SUMO protease family (deSUMOylation) SENP1–SENP5. The y-axis represents the gene expression level in $\text{Log}_2(\text{CPM})$. The plot shows variability in expression levels across the three tissue types, with notable differences in expression between normal muscle and cancerous FP-RMS and FN-RMS tissues. Statistics: **: $p < 0.005$; *: $p < 0.05$

less affected and a comparable reduction in proliferation was only observed after 72 h with 50 nM TAK-981. Control hSKM cells exhibited minimal sensitivity to TAK-981, suggesting its selective inhibition in cancerous cells.

The calculation of the half-maximal inhibitory concentrations (IC_{50}) from dose–response curves for TAK-981 confirmed that FN-RMS lines (RH36, RD12 and RD) were more sensitive to TAK-981 treatment compared to FP-RMS lines (RH30, RH41) and hSKM cells, as shown after 48-h (Supplementary Fig. 3B) and 72-h (Fig. 5C) treatments. IC_{50} values for a 72-h treatment corresponded to 8.01, 9.86 and 32.73 nM for RH36, RD12 and RD lines, respectively, while RH30, RH41 and hSKM cells reaching 88.26, 41.35 and 77.57 nM (Fig. 5C).

To explore the antitumorigenic effects of TAK-981 in both alveolar and embryonal cells, we conducted colony formation assays. A 10% reduction in colony formation was observed in embryonal cells (RH36, RD12 and RD) at 1 nM TAK-981 ($p < 0.05$), whereas a similar reduction was only detected in alveolar cells (RH30 and RH41) at 10 nM

TAK-981 ($p < 0.05$). At 10 nM TAK-981, the colony formation in embryonal cells was reduced by approximately 50% ($p < 0.001$), while in alveolar cells, the reduction was limited to 10% ($p < 0.05$), indicating lower sensitivity compared to embryonal subtypes. Treatment with 50 nM TAK-981 resulted in a 70–80% reduction in colony formation across all cell lines ($p < 0.001$), (Fig. 5D). Functionally, TAK-981 impairs cell migration, proliferation, and colony formation in RMS cells, with embryonal RMS cells showing greater sensitivity than alveolar RMS cells. Minimal effects on control hSKM cells suggest TAK-981's selective anticancer potential.

TAK-981 sensitizes RMS cells to chemotherapy but not to radiotherapy

We next examined whether TAK-981 could exert a synergistic or additive effect when combined with other chemotherapeutic agents commonly used in RMS therapy, specifically actinomycin D and doxorubicin. The Combination Index (CI) for the simultaneous treatment with TAK-981 and chemotherapeutic agents (Actinomycin D, and Doxorubicin) was calculated by using both the Response Additivity Method and the Bliss Independence Method [46]. Results showed that the combined treatment of TAK-981 and chemotherapeutic agents appears to be mostly additive for all RMS cells, with CI values ranging from 1.42 to 0.67 (Table 2).

Importantly, effects in cell viability after 48 h were observed in combination with 10 μM TAK-981 and 0.5 μM actinomycin D or 0.5 μM doxorubicin for RH30 ($p < 0.001$; $p < 0.05$), RH41 ($p < 0.001$; $p < 0.05$), RH36 ($p < 0.001$; $p < 0.001$), RD12 ($p < 0.001$; $p < 0.001$), and RD ($p < 0.001$; $p < 0.001$), (Fig. 6A).

To enhance the evaluation of TAK-981's therapeutic potential in combination with chemotherapeutic agents, we conducted proliferation assays in which RMS cells were treated for 24 and 48 h with 0.5 μM actinomycin D or 0.5 μM doxorubicin, alone or combined with 1 or 10 μM TAK-981. The combination treatment resulted in a significant reduction in cell proliferation as early as 24 h ($p < 0.05$; $p < 0.001$), indicating a prevalently cytotoxic effect across all RMS cell lines tested (Supplementary Fig. 4).

To investigate whether TAK-981 also influences radiosensitivity, we treated the RMS cell lines with varying concentrations of TAK-981, followed by irradiation (Fig. 6B). Colony formation assays revealed no significant differences in survival fractions between cells treated with TAK-981 alone and those treated with TAK-981 followed by irradiation at any concentration tested. These results indicate that TAK-981 did not enhance radiosensitivity in RMS cells. These data suggest that TAK-981 is a potent inhibitor of SUMO conjugation that demonstrates antitumor activity both as a

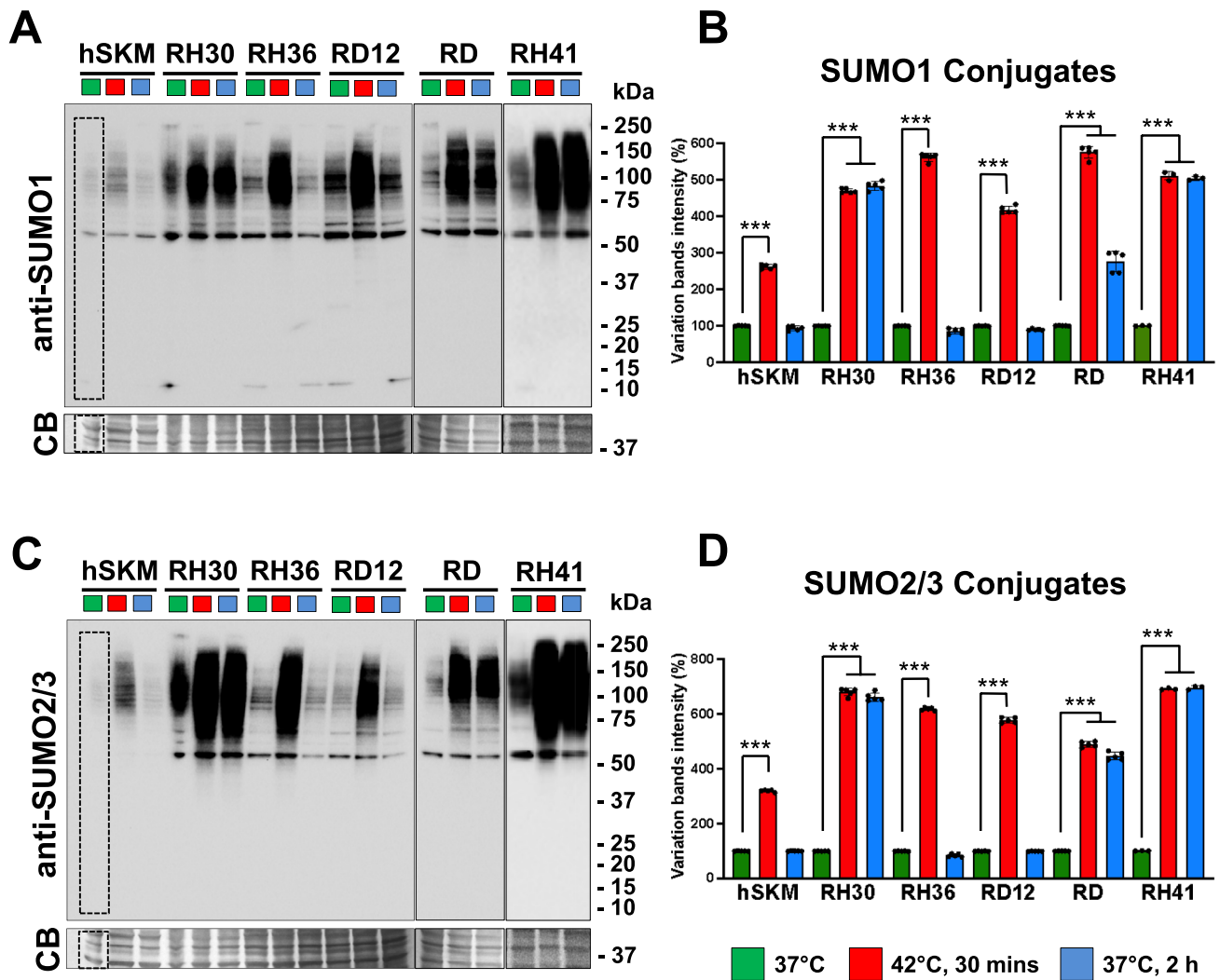


Fig. 3 Heat shock and recovery treatments of RMS cells. Lysates of hSKM and RMS cells grown at 37 °C (green color), at 42 °C for 30 min (red color) and then replaced at 37 °C (blue color) for 2 h were separated in SDS-Page gels and membranes probed with anti-SUMO1 (A) and anti-SUMO2/3 antibodies (C). Band intensity quantification of the SUMO1 (B) and SUMO2/3 (D) conjugates were

determined within the dashed areas, normalized to the total loading protein (Coomassie blue—CB) and expressed as percentages relative to sample grown at 37 °C (green color). Molecular weight markers (kDa) are indicated on the right. All data were presented as mean \pm standard deviation from five independent experiments, except for RH41, $n=3$. Statistics: ***: $p<0,001$

monotherapy and in combination with other chemotherapeutic agents in both alveolar and embryonal RMS subtypes.

TAK-981 inhibits AKT, ERK, and CAV1 phosphorylation

Since AKT, ERK, and caveolin-1 (CAV1) are key regulators of cell migration and proliferation [47, 48], we investigated the impact of TAK-981 on their activation states [49–51]. TAK-981 caused a significant reduction in phosphorylated AKT (p-AKT), resulting in a greater than 50% decrease in RH41, RH36, RD12 and RD cells at 1 nM ($p<0.001$), (Fig. 7A). RH30 and hSKM cells were less sensitive with

relevant reduction of AKT phosphorylation being only apparent at 50 nM, ($p<0.001$). Total AKT levels were unaffected. Similarly, total ERK levels remained stable, while p-ERK was reduced by > 80% in RD12 and hSKM cells at 10 nM ($p<0.001$), and in RH36 and RD cells at 50 nM ($p<0.001$), while in RH41 at 1 nM ($p<0.001$), (Fig. 7B). In RH30 cells, a 70% reduction in p-ERK required 100 nM of TAK-981 ($p<0.001$). Interestingly, ERK phosphorylation was most sensitive in hSKM and RD12 cells, indicating that the sensitivity of SUMO effects on the different downstream pathways is cell type specific.

Phosphorylated CAV1 (p-CAV1) was only detected in RH30, RH41 and weakly in RD cells. In RD, p-CAV1

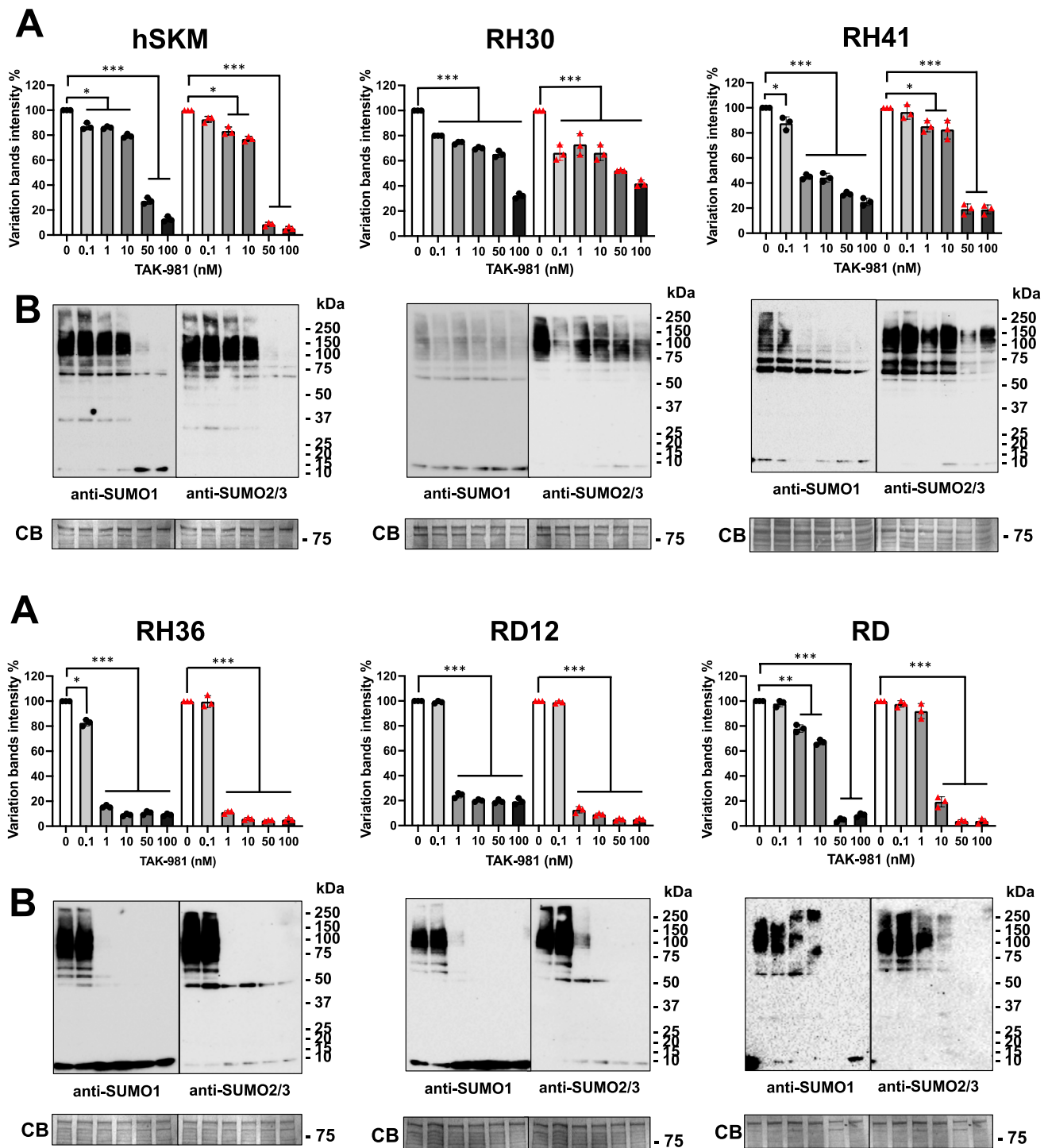


Fig. 4 Impact of TAK-981 on SUMOylation, cell migration, proliferation and colony formation in RMS and control cells. **A** Quantification of global SUMOylation in hSKM (human skeletal muscle) cells and four RMS cell lines (RH30, RH41, RH36, RD12, and RD) following treatment with increasing concentrations of TAK-981 (0, 0.1, 1, 10, 50, and 100 nM). Data are expressed as the percentage of variation in band intensity compared to control (0 nM). Black symbols refer to SUMO1 and red symbols to SUMO2/3 conjugates. **B** Western

blot of SUMO1 and SUMO2/3-conjugated proteins in hSKM, RH30, RH36, RD12, and RD cells treated with TAK-981. The blots demonstrate the drug effects on SUMO1 and SUMO2/3 conjugation. CB refers to Coomassie Blue staining, used as a loading control. Molecular weight markers (kDa) are indicated on the right. All data were presented as the mean \pm standard deviation from three independent experiments. Statistics: *: $p > 0.05$; **: $p > 0.005$; ***: $p < 0.001$

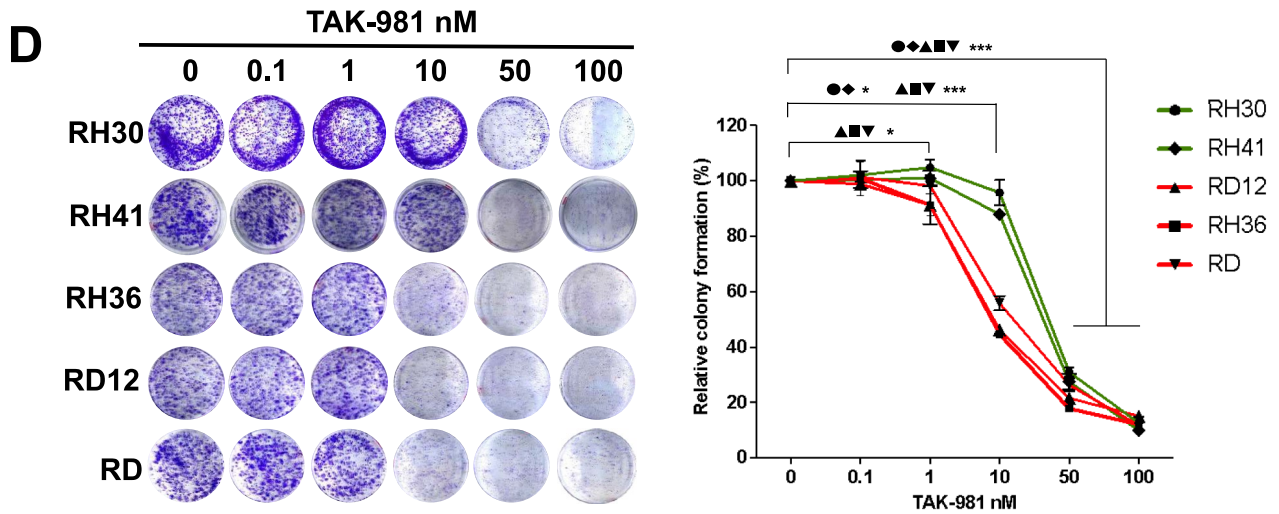
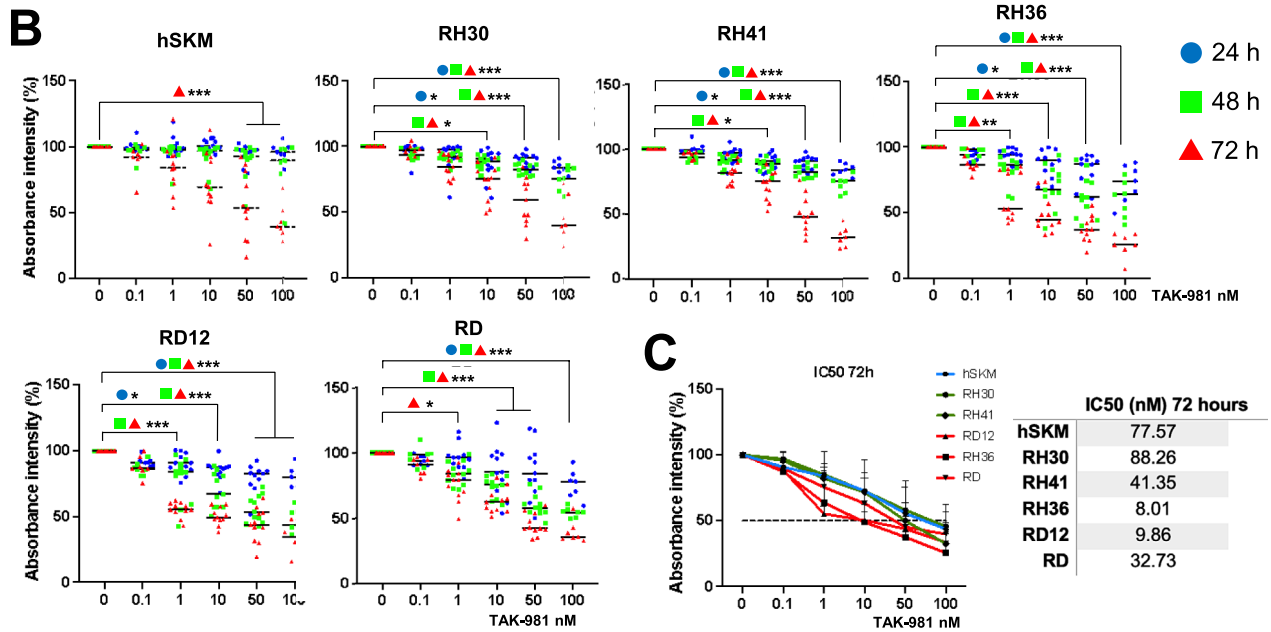
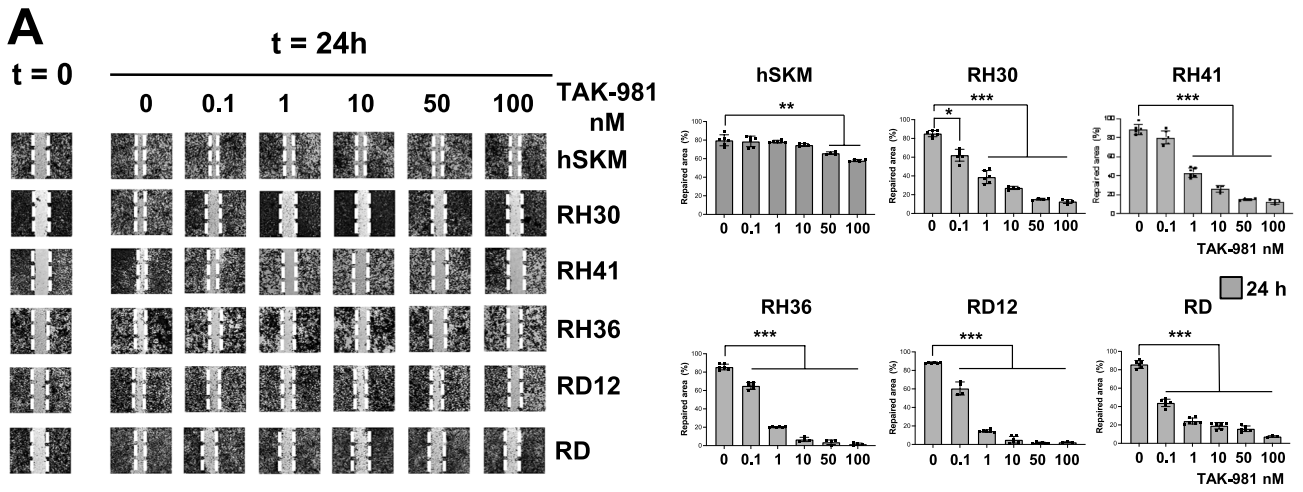


Fig. 5 Impact of TAK-981 on cell migration, proliferation and colony formation in RMS and control cells. **A** Representative images from the wound healing assay. Migration percentage was quantified at time 0 and 24 h for hSKM and RMS cell lines (RH30, RH41, RH36, RD12, and RD) treated with TAK-981 at the indicated concentrations. Images show the progression of wound closure, with the dashed lines marking the wound edges at $t=0$. Cell migration percentage was quantified 24 h after treatment. Average and standard deviations are calculated for $n=6$ independent experiments. Statistics: *: $p<0.05$; **: $p<0.005$; ***: $p<0.001$. **B** Cell proliferation was measured by absorbance intensity in hSKM, RH30, RH41, RH36, RD12, and RD cells treated with increasing concentrations of TAK-981 (0, 0.1, 1, 10, 50, and 100 nM) for 24 (blue symbols), 48 (green symbols), and 72 (red symbols) hours. The colored symbols represent the individual data for the different time points, and bars indicate the mean of $n=12$ independent experiments. Statistics: *: $p<0.05$; **: $p<0.005$; ***: $p<0.001$. **C** Dose response curves used to calculate the IC_{50} doses of TAK-981. RMS and hSKM lines were treated with doses of TAK-981 ranging from 0.1 to 100 nM for 72 h. The black dotted line corresponds to the 50% inhibition. The IC_{50} values are shown in the right table. **D** Colony formation assay results with quantitative analysis. RMS cell lines (RH30, RH41, RH36, RD12, and RD) were treated with increasing concentrations of TAK-981 (0, 0.1, 1, 10, 50, and 100 nM). Representative images of colonies stained with crystal violet are shown for each cell line and treatment condition. The graph on the right showed the quantification of colony formation relative to control (0 nM TAK-981), with data expressed as a percentage. All data were presented as the mean \pm standard deviation from three independent experiments. Statistics: *: $p<0.05$; **: $p<0.005$; ***: $p<0.001$

was undetectable at 10 nM TAK-981 ($p<0.001$), while in RH30 and RH41, $>60\%$ reduction was observed with 50 nM ($p<0.001$). In RH36 and RD12 cells, where p-CAV1 was absent, total CAV1 protein levels decreased by $\sim 50\%$ at 50 nM TAK-981, and by the same percentage in hSKM cells at 100 nM ($p<0.001$), (Fig. 7C). Thus, TAK-981 effectively inhibited the phosphorylation of AKT, ERK, and CAV1 in a dose-dependent manner in different RMS cell lines with subtype-specific sensitivity profiles, demonstrating its potential as a therapeutic agent targeting multiple signaling pathways.

Table 2 For each cell line, Combination Index (CI) values were determined for co-treatment with TAK-981 (TAK) at 1 or 10 μ M in combination with either 0.5 nM actinomycin D (ActD) or 0.5 μ M doxorubicin (DOX)

	Combination Index							
	Response Additivity Method				Bliss Independence Method			
	TAK 1 + ActD 0.5	TAK 10 + ActD 0.5	TAK 1 + DOX 0.5	TAK 10 + DOX 0.5	TAK 1 + ActD 0.5	TAK 10 + ActD 0.5	TAK 1 + DOX 0.5	TAK 10 + DOX 0.5
RH30	1.35	0.93	1.26	1.10	1.23	0.82	1.14	0.95
RH41	1.21	1.07	1.18	1.17	1.10	0.91	1.07	0.99
RH36	0.85	0.86	0.83	0.80	1.00	0.79	0.98	0.73
RD12	1.08	0.83	1.14	0.83	1.05	0.75	1.11	0.73
RD	1.42	0.76	0.91	0.90	1.31	0.67	0.83	0.79

CI values were calculated using the Response Additivity and Bliss Independence models following 48 h of treatment

Discussion

This study underscores the pivotal role of SUMOylation in defining the pathophysiology of RMS and highlights its broader implications for tumor behavior, stress responses, and therapeutic intervention. It is reasonable to infer that elevated levels of SUMO, along with E1, E2 or E3 enzymes lead to increased SUMOylated proteins. Conversely, higher levels of deSUMOylating enzymes may enhance the reduction of SUMO conjugates. Since maintaining the SUMOylation equilibrium is crucial for all cells, alterations in the SUMO pathway components has been described as a mechanism driving neoplastic diseases [21].

Our findings reveal significantly elevated levels of SUMO1 and SUMO2/3 conjugates in RMS cell lines, particularly in RH30 and RH41 (FP-RMS) and RH36, RD12, and RD (FN-RMS) cells, compared to commercial primary human skeletal muscle (hSKM) from adult donors. A limitation of this study is the lack of an appropriate control, as primary human skeletal muscle from children would be more suitable, given that RMS is a pediatric tumor, and gene expression profiles can differ significantly between pediatric and adult tissues; however, we have applied for ethical approval for the use of human tissues in our future studies.

The observed upregulated SUMOylation likely drives tumor progression through its effects on key cellular processes such as DNA repair, transcription, and cell cycle regulation [20, 45].

Transcriptomic analyses reveal that the varying levels of SUMOylation among RMS cell subtypes are attributable to differential expression of SUMO enzymes. This heterogeneity underscores subtype-specific dependencies on the SUMOylation machinery. Alveolar and embryonal RMS cells appear to leverage upregulated SUMOylation to adapt to distinct oncogenic pressures, emphasizing the role of SUMOylation in shaping tumor phenotype and behavior.

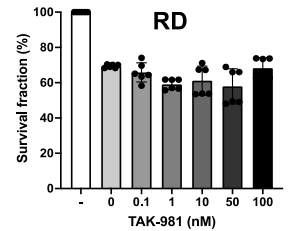
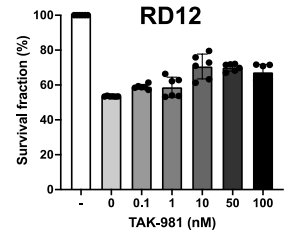
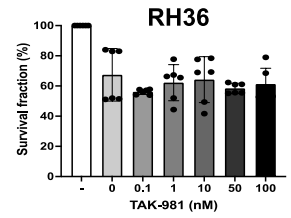
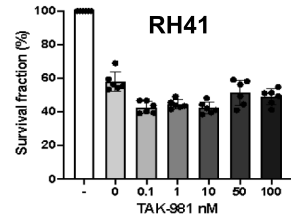
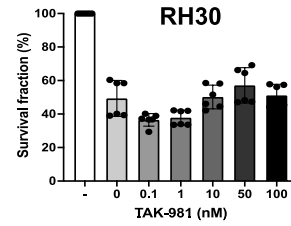
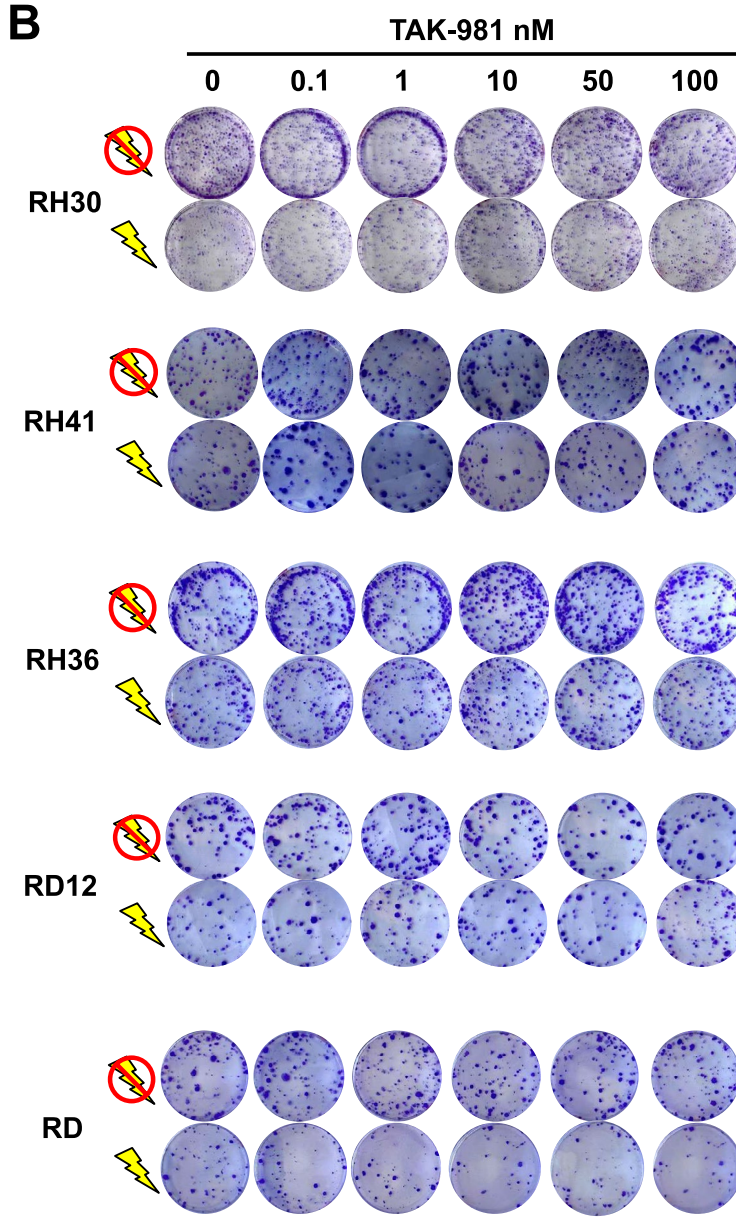
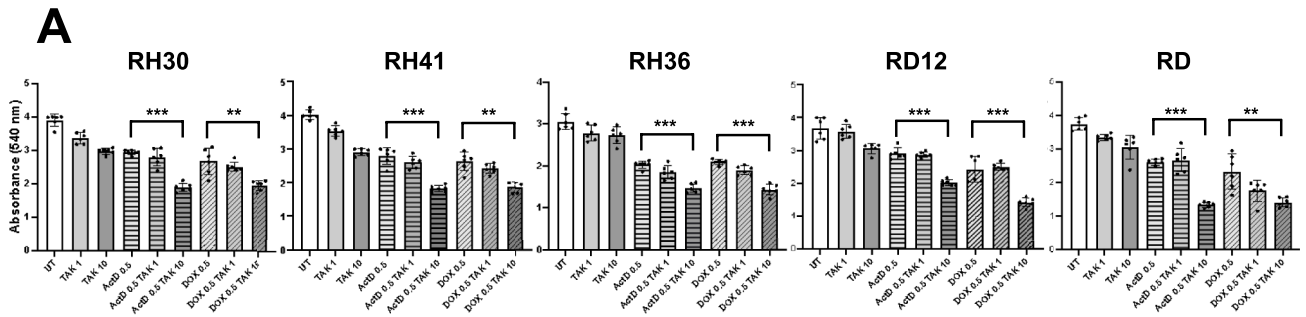


Fig. 6 TAK-981 enhances the efficacy of chemotherapy when combined with other drugs but does not influence radiosensitivity. **A** RH30, RH41, RH36, RD12, and RD were treated with TAK-981 alone or in combination with chemotherapeutic agents (Actinomycin D, ActD, or Doxorubicin, DOX). Bar graphs show cell viability measured by absorbance at 540 nm under different treatment conditions: untreated (UT), TAK-981 (1 nM, 10 nM), ActD (0.5 nM), DOX (0.5 μ M), and combination treatments. Each bar represents mean \pm SD from $n=6$ replicates, and results indicate that TAK-981 alone and in combination with ActD or DOX reduces cell viability in all tested RMS cell lines. Statistics: **: $p < 0.005$; ***: $p < 0.001$. **B** Clonogenic survival assay of RMS cell lines after TAK-981 treatment with and without irradiation. Colony formation in RMS cell lines (RH30, RH41, RH36, RD12, and RD) treated with increasing concentrations of TAK-981 (0, 0.1, 1, 10, 50, 100 nM) both in the presence (lightning symbol) and absence (no symbol) of radiation. Cells were stained with crystal violet to visualize colonies. Quantification of the survival fraction (percentage of surviving colonies) after treatment with TAK-981 and irradiation in RH30, RH41, RH36, RD12, and RD cell lines. Bars represent the mean survival fraction \pm standard deviation across different TAK-981 concentrations of $n=6$ independent experiments

The overexpression of SAE1, a component of the SUMO E1 enzyme and a potential biomarker of this cancer type, along with SUMO maturation-specific proteases SENP1 and SENP3 [17], was consistent across all RMS cells and tumor samples analyzed. Despite the downregulation of several SUMO pathway components such as UBA2, UBC9, and PIAS1, the upregulation of SAE1 in RMS may act as a key driver of upregulated SUMOylation by enhancing the initial activation step of the SUMOylation cascade. Increased expression of SUMO proteases could reflect a compensatory response or contribute to SUMO recycling, indirectly supporting sustained SUMOylation. Overall, the imbalance suggests a reprogramming of SUMO dynamics, with SAE1 playing a central role in promoting elevated SUMOylation in RMS.

Together with its role in tumor progression, altered SUMOylation impacts cellular stress responses. For example, RH30 and RD cells exhibit an aberrant SUMOylation response to heat shock, maintaining elevated levels of SUMO-conjugated proteins even after heat shock recovery, in stark contrast to normal skeletal muscle. This persistent SUMOylation likely enhances RMS cells' ability to survive under stress, facilitating tumor adaptation and progression. The differential stress responses among RMS subtypes highlight the complexity of SUMO-dependent regulatory mechanisms and their role in tumor resilience.

The centrality of SUMOylation in RMS pathophysiology makes the SUMO pathway a compelling therapeutic target. TAK-981, a potent SUMOylation inhibitor that binds to SAE1, effectively impaired tumorigenic processes such as proliferation, migration, and colony formation in RMS cells, demonstrating its potential as a monotherapy or adjunct in RMS treatment. Interestingly, the differential sensitivity of RMS subtypes to TAK-981 highlights

the complexity of SUMOylation's role in tumor biology. Embryonal RMS cells showed greater sensitivity to TAK-981 than alveolar RMS cells, with RH30 cells exhibiting partial resistance. These findings necessitate further exploration of subtype-specific SUMO dependencies to optimize therapeutic strategies. A key finding of this study is the ability of TAK-981 to enhance the efficacy of commonly used chemotherapeutic agents, such as actinomycin D and doxorubicin, in RMS cell lines, although its lack of impact on radiosensitivity highlights a nuanced limitation.

This result aligns with previous reports showing that TAK-981 amplifies the effect of rituximab in promoting innate immune responses [52] and synergizes with 5-azacytidine in the preclinical acute myeloid leukemia treatment [40]. The observed additive effect, where TAK-981 in combination with actinomycin D and doxorubicin drugs resulted in greater inhibition of cell proliferation compared to monotherapy, underscores its potential as an adjunct to chemotherapy in RMS treatment. This is particularly relevant for RMS, where treatment resistance and recurrence remain significant clinical challenges. The synergy observed with chemotherapy may arise from SUMO's influence on transcriptional and DNA repair pathways, which are differently involved in radiation-induced damage responses. Indeed, cells undergoing active proliferation are typically the most susceptible to radiation-induced damage. Consequently, a drug that inhibits cell proliferation may not necessarily enhance sensitivity to radiotherapy.

The impact of SUMOylation inhibition extends beyond direct tumorigenic effects to the modulation of key signaling pathways. TAK-981's ability to reduce phosphorylation of AKT, ERK, and CAV1 underscores its broad regulatory role in cellular survival and proliferation pathways. This multi-faceted mechanism suggests that targeting SUMOylation not only disrupts tumor growth but also alters the signaling networks that sustain oncogenic phenotypes.

However, the overarching dysregulation of SUMO enzymes (e.g., overexpression of SAE1, SENPs, and reduced UBA2) presents additional avenues for genetic intervention. These molecular imbalances correlate with poor survival outcomes, reinforcing the prognostic and therapeutic value of targeting SUMO components.

In RMS, key oncogenic proteins such as PAX3/7-FOXO1 [31, 32] and MDM2 [53] undergo SUMOylation, which enhances their stability, localization, and transcriptional activity, contributing to tumor progression. This post-translational modification supports oncogenic signaling and impairs tumor suppressor pathways, highlighting the SUMOylation machinery as a mechanistically relevant and promising therapeutic target in RMS.

In this study, we provide solid evidence that SUMOylation emerges as a cornerstone of RMS pathophysiology,

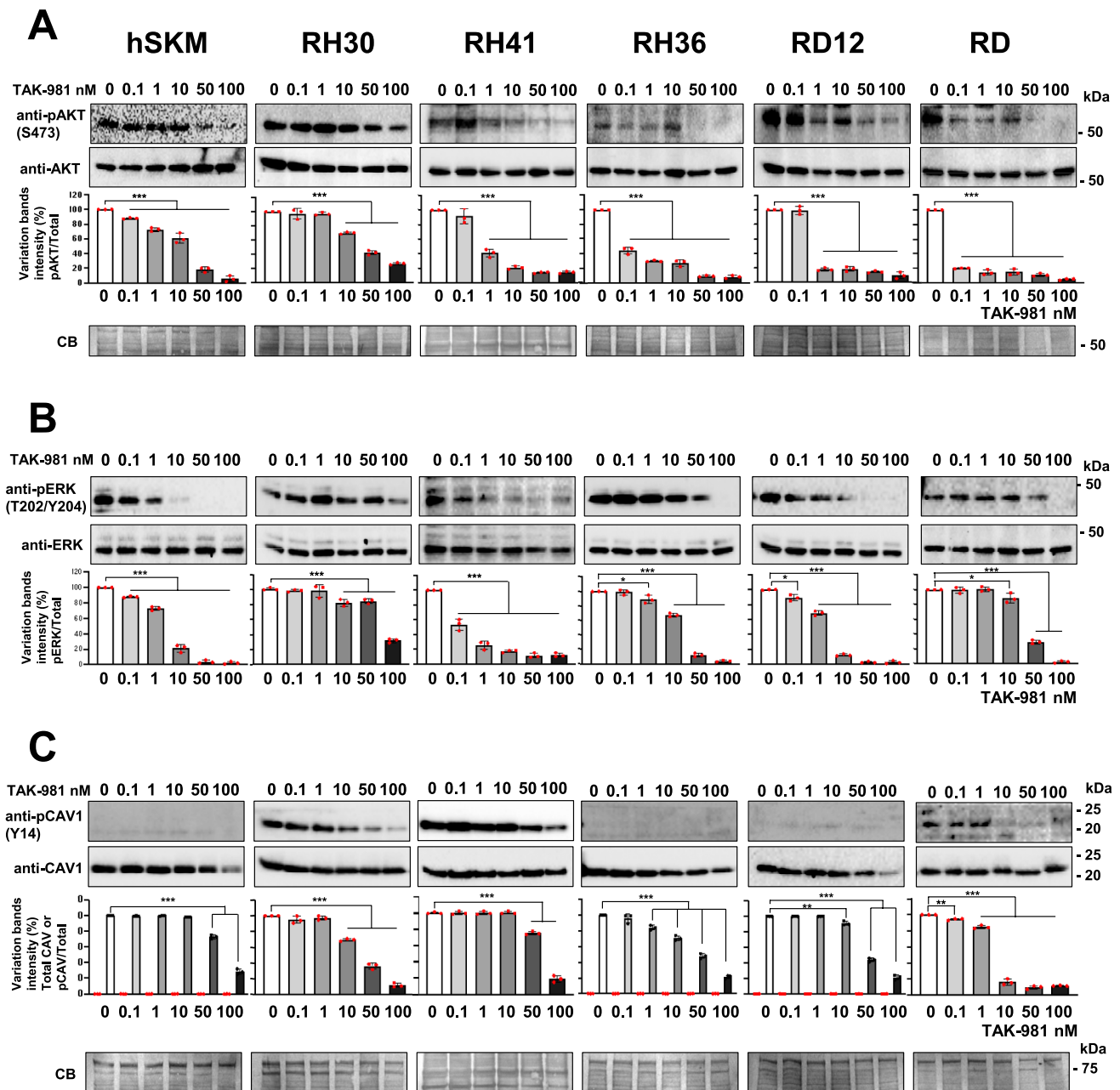


Fig. 7 TAK-981 inhibits key signaling pathways in RMS cell lines after 72 h of treatment. **A** Western blot showing the dose-dependent inhibition of AKT (phosphorylated AKT, S473) levels upon treatment with TAK-981 in a panel of RMS cell lines (RH30, RH41, RH36, RD12, RD) and control hSKM (human skeletal muscle cells). Cells were treated with TAK-981 at concentrations of 0, 0.1, 1, 10, 50, and 100 nM. Blots were probed with antibodies against pAKT (Ser473) and total AKT. The intensity of pAKT bands is progressively reduced in most cell lines, indicating the TAK-981 ability to downregulate AKT activation. The corresponding histograms below the blots depict the quantification of pAKT/total AKT (red symbols), showing the relative levels at different concentrations of TAK-981 and referred to the vehicle (0 nM) treatment. Statistics: **: $p < 0.005$; ***: $p < 0.001$. **B** Western blots showing the effect of TAK-981 on ERK phosphorylation (pERK, T202/Y204) in the same panel of cell lines. Antibodies against pERK and total ERK were used. TAK-981 treatment leads

to a dose-dependent reduction in pERK levels across most cell lines, as seen in the blot intensities. The quantification (bar graphs below) illustrates the pERK/total ERK levels (red symbols) at different concentrations of TAK-981 and referred to the vehicle (0 nM) treatment. Statistics: *: $p < 0.05$; **: $p < 0.005$; ***: $p < 0.001$. **C** Western blots demonstrating the effect of TAK-981 on phosphorylated CAV1 (pCAV1, Y14) and total CAV1 in RMS cell lines and hSKM cells. The cells were treated with the same doses of TAK-981 (0, 0.1, 1, 10, 50, 100 nM). Quantification of the phosphorylated CAV1/total CAV1 (red symbols) and total CAV1 (black symbols) is shown in the bar graphs below. Statistics: **: $p < 0.005$; ***: $p < 0.001$. The loading control for the Western blots is shown as Coomassie Blue staining of total protein. Molecular weight markers (kDa) are indicated on the right. All data were presented as the mean \pm standard deviation from three independent experiments,

orchestrating tumor progression, stress response, and therapeutic resistance. The dysregulation of SUMOylation in RMS, combined with its subtype-specific nuances, highlights its importance as both a biological hallmark and a therapeutic target.

While TAK-981 demonstrates promise as a SUMOylation inhibitor with potent anticancer activity [38, 39, 54], it is recently being tested in combination with other drugs to treat people who have select advanced or metastatic solid tumors of non-squamous non-small-cell lung cancer (NSCLC) or microsatellite-stable colorectal cancer (MSS-CRC), (Clinical trial information: NCT04381650). However, within the range of TAK-981 concentrations (0.1–100 nM) employed in our *in vitro* experiments, the calculated IC_{50} after 72 h of treatment were between 41.35 and 88.26 nM for FP-RMS and 8.01–32.73 nM for FN-RMS, resulting in lower concentrations than previous pre-clinical studies in different cancer models such as U937, THP-1 where the observed IC_{50} was between 118 and 157 nM respectively, after 24 h of treatment [40]. Phase I clinical trials of TAK-981 are ongoing for various tumor types [30]; notably, the maximum plasma concentration achieved at the recommended Phase II dose in human cancers exceeds 1 μ M [55].

For RMS, further investigation into the molecular intricacies of the SUMO pathway and mechanisms of drug resistance is crucial. Our findings support the integration of SUMO-targeted therapies with existing treatment modalities, emphasizing the need for subtype-specific approaches. By advancing our understanding of SUMOylation in RMS, we further aim to characterize and identify the SUMO1 and SUMO2/3 targets by Mass Spectrometry analysis, and develop more effective and personalized interventions, addressing the persistent challenges of treatment resistance and recurrence in this aggressive malignancy. Indeed, in cancer, these differences translate into distinct signaling consequences: SUMO1 is commonly associated with the stabilization and activation of oncogenic transcription factors (e.g., c-Myc, mutant p53), promoting tumor growth and survival. Conversely, SUMO2/3 play a more dynamic role in cellular stress responses, DNA repair, and proteostasis making them particularly relevant in cancer survival and adaptation. Their poly-SUMO chains can recruit SUMO-targeted ubiquitin ligases (STUbLs), linking SUMOylation to protein degradation pathways, which can either suppress or support tumor progression depending on the cellular context. These isoform-specific functions highlight the nuanced role of SUMOylation in cancer and suggest that therapeutic strategies targeting the SUMO pathway must consider the distinct contributions of SUMO1 and SUMO2/3.

Conclusions

This study highlights SUMOylation as a critical driver of RMS pathophysiology, influencing tumor progression, stress response, and therapeutic resistance. The upregulated SUMOylation and dysregulated SUMO enzymes underscore subtype-specific vulnerabilities. TAK-981 shows promise in inhibiting tumorigenic processes and enhancing chemotherapy, highlighting SUMOylation as a therapeutic target. Further investigation into SUMO pathways dynamics and mechanisms of drug resistance is essential to optimize RMS therapies.

Supplementary Information The online version contains supplementary material available at <https://doi.org/10.1007/s11010-025-05336-6>.

Acknowledgements The contribution of Nairong Liu during the revision of this manuscript is gratefully acknowledged.

Author contributions S.C., E.V.C., S.G. performed the experiments. V.M.L. performed bioinformatic analysis and calculations. S.C., S.G. analyzed the data. All authors contributed to the final version of the manuscript. The study was conceived and supervised by SG.

Funding Open access funding provided by Karolinska Institute. Erik och Edith Fernströms foundation 2022-00596 to SG. KI fund 2022-02802 to SG. Visiting professor grant UniBS 2023-0259542 to SG. Fondazione Umberto Veronesi to SC.

Data availability No datasets were generated or analysed during the current study.

Declarations

Competing interests V.M.L. is CEO and shareholder of HepaPredict AB, as well as shareholder and co-founder of Shanghai Hepo Biotechnology Ltd.

Ethical approval Not applicable.

Consent for publication Not applicable.

Consent to participate Not applicable.

Open Access This article is licensed under a Creative Commons Attribution 4.0 International License, which permits use, sharing, adaptation, distribution and reproduction in any medium or format, as long as you give appropriate credit to the original author(s) and the source, provide a link to the Creative Commons licence, and indicate if changes were made. The images or other third party material in this article are included in the article's Creative Commons licence, unless indicated otherwise in a credit line to the material. If material is not included in the article's Creative Commons licence and your intended use is not permitted by statutory regulation or exceeds the permitted use, you will need to obtain permission directly from the copyright holder. To view a copy of this licence, visit <http://creativecommons.org/licenses/by/4.0/>.

References

1. Skapek SX, Ferrari A, Gupta AA, Lupo PJ, Butler E, Shipley J et al (2019) Rhabdomyosarcoma. *Nat Rev Dis Primers* 5(1):1
2. Shern JF, Chen L, Chmielecki J, Wei JS, Patidar R, Rosenberg M et al (2014) Comprehensive genomic analysis of rhabdomyosarcoma reveals a landscape of alterations affecting a common genetic axis in fusion-positive and fusion-negative tumors. *Cancer Discov* 4(2):216–231
3. Shern JF, Selve J, Izquierdo E, Patidar R, Chou HC, Song YK et al (2021) Genomic classification and clinical outcome in rhabdomyosarcoma: a report from an international consortium. *J Clin Oncol* 39(26):2859–2871
4. Barr FG (1997) Molecular genetics and pathogenesis of rhabdomyosarcoma. *J Pediatr Hematol Oncol* 19(6):483–491
5. Marshall AD, Grosveld GC (2012) Alveolar rhabdomyosarcoma - The molecular drivers of PAX3/7-FOXO1-induced tumorigenesis. *Skelet Muscle* 2(1):25
6. Perez EA, Kassira N, Cheung MC, Koniaris LG, Neville HL, Sola JE (2011) Rhabdomyosarcoma in children: a SEER population based study. *J Surg Res* 170(2):e243–e251
7. O'Brien D, Jacob AG, Qualman SJ, Chandler DS (2012) Advances in pediatric rhabdomyosarcoma characterization and disease model development. *Histol Histopathol* 27(1):13–22
8. Meyer WH, Spunt SL (2004) Soft tissue sarcomas of childhood. *Cancer Treat Rev* 30(3):269–280
9. Miwa S, Yamamoto N, Hayashi K, Takeuchi A, Igarashi K, Tsuchiya H (2020) Recent Advances and challenges in the treatment of rhabdomyosarcoma. *Cancers (Basel)* 12(7):2865
10. Chen C, Dorado Garcia H, Scheer M, Henssen AG (2019) Current and future treatment strategies for rhabdomyosarcoma. *Front Oncol* 9:1458
11. Bergeron C, Jenney M, De Corti F, Gallego S, Merks H, Glosli H et al (2021) Embryonal rhabdomyosarcoma completely resected at diagnosis: The European paediatric Soft tissue sarcoma Study Group RMS2005 experience. *Eur J Cancer* 146:21–29
12. Guo D, Li M, Zhang Y, Yang P, Eckenrode S, Hopkins D et al (2004) A functional variant of SUMO4, a new I kappa B alpha modifier, is associated with type 1 diabetes. *Nat Genet* 36(8):837–841
13. Owerbach D, McKay EM, Yeh ET, Gabbay KH, Bohren KM (2005) A proline-90 residue unique to SUMO-4 prevents maturation and sumoylation. *Biochem Biophys Res Commun* 337(2):517–520
14. Liang YC, Lee CC, Yao YL, Lai CC, Schmitz ML, Yang WM (2016) SUMO5, a Novel Poly-SUMO Isoform. Regulates PML Nuclear Bodies *Sci Rep* 6:26509
15. Geiss-Friedlander R, Melchior F (2007) Concepts in sumoylation: a decade on. *Nat Rev Mol Cell Biol* 8(12):947–956
16. Kerscher O, Felberbaum R, Hochstrasser M (2006) Modification of proteins by ubiquitin and ubiquitin-like proteins. *Annu Rev Cell Dev Biol* 22:159–180
17. Nayak A, Muller S (2014) SUMO-specific proteases/isopeptidases: SENPs and beyond. *Genome Biol* 15(7):422
18. Gong L, Millas S, Maul GG, Yeh ET (2000) Differential regulation of sentrinized proteins by a novel sentrin-specific protease. *J Biol Chem* 275(5):3355–3359
19. Celen AB, Sahin U (2020) Sumoylation on its 25th anniversary: mechanisms, pathology, and emerging concepts. *FEBS J* 287(15):3110–3140
20. Flotho A, Melchior F (2013) Sumoylation: a regulatory protein modification in health and disease. *Annu Rev Biochem* 82:357–385
21. Seeler JS, Dejean A (2017) SUMO and the robustness of cancer. *Nat Rev Cancer* 17(3):184–197
22. Subramonian D, Raghunayakula S, Olsen JV, Beningo KA, Paschen W, Zhang XD (2014) Analysis of changes in SUMO-2/3 modification during breast cancer progression and metastasis. *J Proteome Res* 13(9):3905–3918
23. Wu YJ, Huang ST, Chang YH, Lin SY, Lin WL, Chen YJ et al (2023) SUMO-activating enzyme subunit 1 is associated with poor prognosis, tumor progression, and radio-resistance in colorectal cancer. *Curr Issues Mol Biol* 45(10):8013–8026
24. Wang Y, Yu J (2021) Dissecting multiple roles of SUMOylation in prostate cancer. *Cancer Lett* 521:88–97
25. Ke C, Zhu K, Sun Y, Ni Y, Zhang Z, Li X (2019) SUMO1 promotes the proliferation and invasion of non-small cell lung cancer cells by regulating NF-kappaB. *Thorac Cancer* 10(1):33–40
26. Wu X, Li JH, Xu L, Li YX, Zhu XX, Wang XY et al (2023) SUMO specific peptidase 3 halts pancreatic ductal adenocarcinoma metastasis via deSUMOylating DKC1. *Cell Death Differ* 30(7):1742–1756
27. Du L, Li YJ, Fakhri M, Wiatrek RL, Duldulao M, Chen Z et al (2016) Role of SUMO activating enzyme in cancer stem cell maintenance and self-renewal. *Nat Commun* 7:12326
28. Lara-Urena N, Jafari V, Garcia-Dominguez M (2022) Cancer-associated dysregulation of sumo regulators: proteases and ligases. *Int J Mol Sci* 23(14):8012
29. Cox OF, Huber PW (2019) Developing practical therapeutic strategies that target protein SUMOylation. *Curr Drug Targets* 20(9):960–969
30. Kroonen JS, Vertegaal ACO (2021) Targeting SUMO signaling to wrestle cancer. *Trends Cancer* 7(6):496–510
31. Luan Z, Liu Y, Stuhlmiller TJ, Marquez J, Garcia-Castro MI (2013) SUMOylation of Pax7 is essential for neural crest and muscle development. *Cell Mol Life Sci* 70(10):1793–1806
32. Zhang X, Ge L, Jin G, Liu Y, Yu Q, Chen W et al (2024) Cold-induced FOXO1 nuclear transport aids cold survival and tissue storage. *Nat Commun* 15(1):2859
33. Hirohama M, Kumar A, Fukuda I, Matsuoka S, Igarashi Y, Saitoh H et al (2013) Spectomycin B1 as a novel SUMOylation inhibitor that directly binds to SUMO E2. *ACS Chem Biol* 8(12):2635–2642
34. Fukuda I, Ito A, Hirai G, Nishimura S, Kawasaki H, Saitoh H et al (2009) Ginkgolic acid inhibits protein SUMOylation by blocking formation of the E1-SUMO intermediate. *Chem Biol* 16(2):133–140
35. Schneeweis C, Hassan Z, Schick M, Keller U, Schneider G (2021) The SUMO pathway in pancreatic cancer: insights and inhibition. *Br J Cancer* 124(3):531–538
36. Kho C, Lee A, Jeong D, Oh JG, Gorski PA, Fish K et al (2015) Small-molecule activation of SERCA2a SUMOylation for the treatment of heart failure. *Nat Commun* 6:7229
37. Lightcap ES, Yu P, Grossman S, Song K, Khattar M, Xega K et al (2021) A small-molecule SUMOylation inhibitor activates antitumor immune responses and potentiates immune therapies in preclinical models. *Sci Transl Med.* 13(611):eaba7791
38. Kim HS, Kim BR, Dao TTP, Kim JM, Kim YJ, Son H et al (2023) TAK-981, a SUMOylation inhibitor, suppresses AML growth immune-independently. *Blood Adv* 7(13):3155–3168
39. Kumar S, Schoonderwoerd MJA, Kroonen JS, de Graaf IJ, Sluiter M, Ruano D et al (2022) Targeting pancreatic cancer by TAK-981: a SUMOylation inhibitor that activates the immune system and blocks cancer cell cycle progression in a preclinical model. *Gut* 71(11):2266–2283
40. Gabellier L, De Toledo M, Chakraborty M, Akl D, Hallal R, Aqrouq M et al (2024) SUMOylation inhibitor TAK-981

- (subasumstat) synergizes with 5-azacytidine in preclinical models of acute myeloid leukemia. *Haematologica* 109(1):98–114
41. Namuduri AV, Heras G, Lauschke VM, Vitadello M, Traini L, Cacciani N et al (2020) Expression of SUMO enzymes is fiber type dependent in skeletal muscles and is dysregulated in muscle disuse. *FASEB J* 34(2):2269–2286
 42. Namuduri AV, Heras G, Mi J, Cacciani N, Hornaeus K, Konzer A et al (2017) A proteomic approach to identify alterations in the small ubiquitin-like modifier (SUMO) network during controlled mechanical ventilation in rat diaphragm muscle. *Mol Cell Proteomics* 16(6):1081–1097
 43. Ge SX, Son EW, Yao R (2018) iDEP: an integrated web application for differential expression and pathway analysis of RNA-Seq data. *BMC Bioinformatics* 19(1):534
 44. Hayes MN, McCarthy K, Jin A, Oliveira ML, Iyer S, Garcia SP et al (2018) Vangl2/RhoA signaling pathway regulates stem cell self-renewal programs and growth in rhabdomyosarcoma. *Cell Stem Cell* 22(3):414–276
 45. Sahin U, de The H, Lallemand-Breitenbach V (2022) Sumoylation in physiology, pathology and therapy. *Cells* 11(5):814
 46. Duarte D, Vale N (2022) Evaluation of synergism in drug combinations and reference models for future orientations in oncology. *Curr Res Pharmacol Drug Discov* 3:100110
 47. Guo YJ, Pan WW, Liu SB, Shen ZF, Xu Y, Hu LL (2020) ERK/MAPK signalling pathway and tumorigenesis. *Exp Ther Med* 19(3):1997–2007
 48. Codenotti S, Faggi F, Ronca R, Chiodelli P, Grillo E, Guescini M et al (2019) Caveolin-1 enhances metastasis formation in a human model of embryonal rhabdomyosarcoma through Erk signaling cooperation. *Cancer Lett* 449:135–144
 49. Lin CH, Liu SY, Lee EH (2016) SUMO modification of Akt regulates global SUMOylation and substrate SUMOylation specificity through Akt phosphorylation of Ubc9 and SUMO1. *Oncogene* 35(5):595–607
 50. Vidal S, Bouzaher YH, El Motiam A, Seoane R, Rivas C (2022) Overview of the regulation of the class IA PI3K/AKT pathway by SUMO. *Semin Cell Dev Biol* 132:51–61
 51. Lorente M, Garcia-Casas A, Salvador N, Martinez-Lopez A, Gabicagogeascoa E, Velasco G et al (2019) Inhibiting SUMO1-mediated SUMOylation induces autophagy-mediated cancer cell death and reduces tumour cell invasion via RAC1. *J Cell Sci* 132(20):jcs234120
 52. Nakamura A, Grossman S, Song K, Xega K, Zhang Y, Cvet D et al (2022) The SUMOylation inhibitor subasumstat potentiates rituximab activity by IFN1-dependent macrophage and NK cell stimulation. *Blood* 139(18):2770–2781
 53. Fuchs SY, Lee CG, Pan ZQ, Ronai Z (2002) SUMO-1 modification of Mdm2 prevents its self-ubiquitination and increases Mdm2 ability to ubiquitinate p53. *Cell* 110(4):531
 54. Langston SP, Grossman S, England D, Afroz R, Bence N, Bowman D et al (2021) Discovery of TAK-981, a first-in-class inhibitor of SUMO-activating enzyme for the treatment of cancer. *J Med Chem* 64(5):2501–2520
 55. Kotani H, Oshima H, Boucher JC, Yamano T, Sakaguchi H, Sato S et al (2024) Dual inhibition of SUMOylation and MEK conquers MYC-expressing KRAS-mutant cancers by accumulating DNA damage. *J Biomed Sci* 31(1):68

Publisher's Note Springer Nature remains neutral with regard to jurisdictional claims in published maps and institutional affiliations.

Authors and Affiliations

Silvia Codenotti¹ · Volker M. Lauschke^{2,3,4,5} · Emma V. Casella¹ · Daniel C. Andersson² · Alessandro Fanzani¹ · Stefano Gastaldello²

✉ Stefano Gastaldello
stefano.gastaldello@ki.se

¹ Department of Molecular and Translational Medicine, University of Brescia, Brescia, Italy

² Department of Physiology and Pharmacology, Karolinska Institutet, Stockholm, Sweden

³ Dr Margarete Fischer-Bosch Institute of Clinical Pharmacology, Stuttgart, Germany

⁴ University of Tübingen, Tübingen, Germany

⁵ Department of Pharmacy, the Second Xiangya Hospital, Central South University, Changsha, China